Gridded maps of geological methane emissions and their isotopic signature

Giuseppe Etiope [1,2], Giancarlo Ciotoli [3,1], Stefan Schwietzke [4], Martin Schoell [5]

[1] Istituto Nazionale di Geofisica e Vulcanologia, Sezione Roma 2, Italy
[2] Faculty of Environmental Science and Engineering, Babes Bolyai University, Cluj-Napoca, Romania
[3] Istituto di Geologia Ambientale e Geoingegneria—CNR-IGAG, Roma, Italy
[4] Cooperative Institute for Research in Environmental Sciences, University of Colorado, Boulder, Colorado, USA, and NOAA Earth System Research Laboratory, Global Monitoring Division, Boulder, Colorado, USA.
[5] Gas-Consult Int., Pleasanton, California, USA

Supplement

Supplementary Tables, Figures and Text

S1. Onshore Seeps (OS)

Table S1. Class of CH_4 emission attributed to onshore seeps (excluding mud volcanoes)

Emission (tonnes/y)	1-50	100	500	1000	2000-3000	5000-9000	10000-20000	50000-60000	80000
N. of seeps (tot. 2086)	522	1069	27	419	14	23	9	2	1

S1.1 Evaluation of MV emission factors

MV flux data acquired before 2006, in Azerbaijan, Romania and Italy (Table S2) refer to flux measurements based on the accumulation chamber technique using syringe sampling and laboratory analyses. The data acquired after 2006, refer to measurements based on new accumulation chambers connected to portable gas sensors (semiconductors or laser detectors). It was verified that the flux derivations by discrete syringe sampling strongly underestimate the flux. A series of tests performed in seepage sites, using simultaneously syringe and online sensor techniques (Etiope, unpublished data), revealed that syringe sampling may underestimate the flux up to 90%, especially for high fluxes (e.g., on the same seep, values of 100 and 1000 kg/day were measured by syringe and online sensors, respectively). The good accuracy and repeatability of the closed chamber technique with online sensors, especially those using TDLAS (Tunable Diode Laser Adsorption Spectroscopy) sensors (with uncertainty < 10%) are described by Etiope et al. (2017) and instrumental manuals (www.westsystems.com). Accordingly, the old flux estimates based on syringe sampling are surely significantly underestimated; therefore, they have not been used for the evaluation of the miniseepage emission factor.

Table S2. Measured methane flux data from mud volcanoes

Measurement method	Country	Mud volcano	Investigated area (km^2)	Miniseepage output ($t\ y^{-1}$)	Macroseep output ($t\ y^{-1}$)	Total emission ($t\ y^{-1}$)	Emission factor ($t\ km^{-2}\ y^{-1}$)	References
syringe sampling and lab analyses	Azerbaijan	Dashgil	0.6	442	623	1065	1775	Etiope et al (2004a)
		Kechaldag	0.05	5.8	4	10	196	"
		Bakhar	0.05	5.5	8.4	14	278	"
	Romania	Paclele Mici	0.62	68.4	255	323	522	Etiope et al (2004b)
		Paclele Mari	1.62	77	300	377	233	"
		Fierbatori	0.025	20	17	37	1480	"
	Italy	Maccalube	1.4	374	20	394	281	"
online sensors	Italy	Frisa	0.001	2.8	2	5	4800	Etiope (unpublished)
		Ospitaletto	0.001	0.6	0.8	1	1400	Etiope et al (2007)
		Pineto	0.0025	1.7	1.6	3	1320	Etiope (unpublished)
		Rivalta	0.003	10.8	1.2	12	4000	Etiope et al (2007)
		Regnano	0.006	29	5	34	5667	"
		Nirano	0.01	26.4	6	32	3240	Etiope et al (2007)
		Serra de Conti	0.006	12	7	19	3167	Etiope (unpublished)
		Monor	0.002	13.9	2.1	16	8000	Spulber et al (2010)
		Filias	0.00005	0.1	0.38	0	9600	"
		Porumbeni Mici	0.00004	0.27	0.2	0	11750	"
		Cobatesti	0.00008	0.2	1.4	2	20000	"
		Boz	0.00002	0.01	0.19	0	10000	"
		Beciu	0.005	7.5	182	190	37900	Frunzeti et al (2012)
	Taiwan	Hsing-yang-nyu-hu	0.0004	0.5	1.7	2	5500	Hong et al (2013)
		Gung-shuei-ping	0.005		1.1	1	220	"
		Wu-shan-ding	0.006	30.2	4.8	35	5833	"
	Japan	Murono	0.0049	16	5	21	4286	Etiope et al (2011)
		Gamo	0.001	1.2	1.8	3	3000	"
	China	Dushanzi	0.02	20.1	2.5	23	1130	Zheng et al (2017)

The “online sensor” data of Table S2 have been used to draw a regression line of seepage area vs. miniseepage (Fig. S2). The line equation has been applied to the OS mud volcano dataset, where the area (km^2) was estimated for each MV (as described above). So, for each MV the miniseepage emission has been estimated. The main uncertainty in this procedure is due to the fact that the measured miniseepage data refer to small size MVs (the large MVs of Azerbaijan and Romania were only measured with the old, underestimating syringe method), and the miniseepage vs area correlation may be different compared to large MVs.

From Table S2 data, a statistical relationship between miniseepage and macro-seepage has also been derived (Fig. S3) and the macro-seepage flux component has been attributed to each MV of the OS dataset. It is known from field surveys that the macro- vs. miniseepage correlation actually depends on the size of the MV: bigger (generally more active) MVs have a relatively higher macro-seepage. Therefore, two regression lines were calculated for MVs smaller and larger than 1 km^2, adopting in this case the old data from Azerbaijan and Romania. The emission of each MV is therefore the sum of miniseepage and macro-seepage flux.

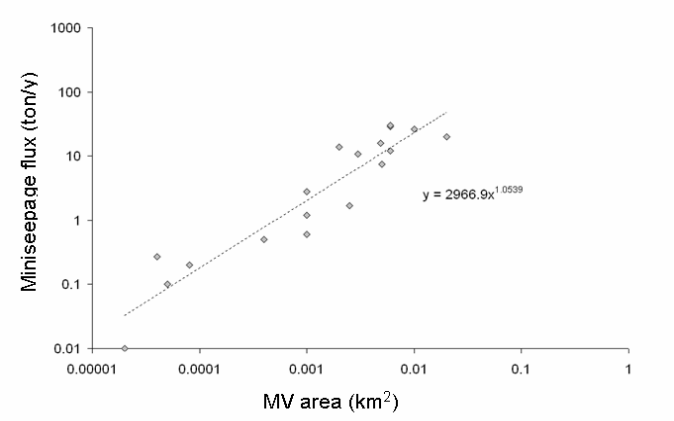

Fig. S2. Correlation between mud volcano area and miniseepage, based on Table S2 data.

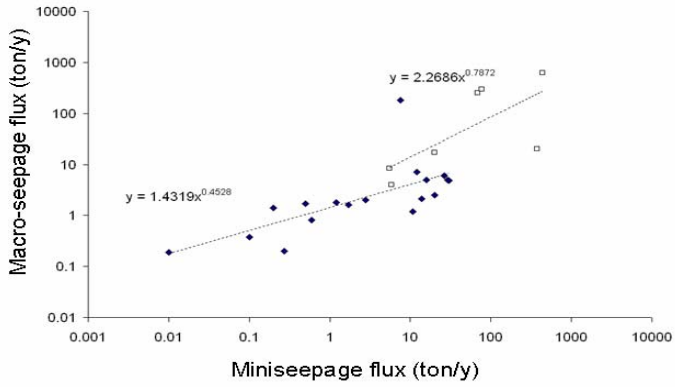

Fig. S3. Correlation between mud volcano miniseepage and macro-seepage, based on Table S2 data. Two regression lines were calculated for MV smaller (blue diamonds) and larger (white squares) than 1 km^2.

Table S3. Extract from the OS dataset showing, as example, the miniseepage flux derived from the area of some mud volcanoes in Azerbaiajn, based on the area vs miniseepage relationship shown in Fig. S2, and miniseepage vs macro-seep flux relationship shown in Fig. S3.

COUNTRY	LAT	LONG	REGION	NAME	area (km2)	minissepage (tonnes/y)	macro-seep (tonnes/y)	Total output (tonnes/y)
Azerbaijan	41.15000	48.93333	Pricaspian	Khanaga	1	2966	1226	4192
Azerbaijan	41.15000	48.93333	Pricaspian	Khydyrzyndy	0.6	1735	42	1777
Azerbaijan	40.71667	49.31667	Pricaspian	Kohna-Gady	0.6	1735	42	1777
Azerbaijan	40.71667	49.31667	Pricaspian	Kurkachidag	1	2966	1226	4192
Azerbaijan	40.98278	49.15917	Pricaspian	Nardaran	0.6	1735	42	1777
Azerbaijan	40.39528	49.88222	Apsheron	Chullutepe	0.4	1133	35	1168
Azerbaijan	40.49389	48.92139	Apsheron	Damlamaja	0.4	1133	35	1168
Azerbaijan	40.39528	49.88222	Apsheron	Girvaalty	0.4	1133	35	1168
Azerbaijan	40.39528	49.88222	Apsheron	Gulbakht	0.4	1133	35	1168
Azerbaijan	40.39528	49.88222	Apsheron	Gullutepe	0.4	1133	35	1168
Azerbaijan	40.47000	49.71700	Apsheron	Kechaldag	1	2966	1226	4192

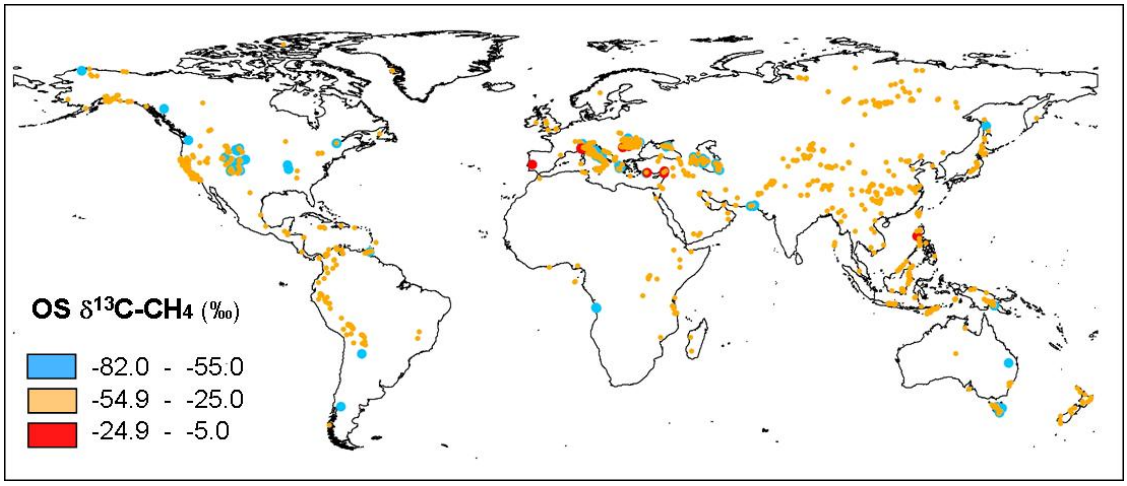

Fig. S4 Distribution of three classes of value of the stable C isotope composition of methane from onshore seeps.

S2. Submarine Seepage (SS)

Table S4. SS dataset developed for gridding. It includes 15 areas where methane output to the atmosphere was estimated, and 16 areas where the emission is unknown.

ID	Country	Seepage area	LAT	LONG	flux (t/y)	area (km^2)	δ^{13}C (‰)	Reference
1	California	Coal Oil Point	34.3953N	119.8825W	30000	3	-43	Hornafius et al 1999
2	Denmark	Kattegat coast	57.45N	10.84E	50	25000	*-60*	Dando et al 1994
3	UK	UK North Sea shelf	52.62N	2.42E	600000	600000	*-60*	Judd et al 1997, Tizzard 2008
4	Spain	Rias Baixas	42.22N	8.84W	11400	751	*-65*	Garcia-Gil 2003
5	Bulgaria-Georgia-Russia-Ukraine-Turkey	Black Sea shelf and coasts	five different zones		920000	132200	*-50*	Dimitrov and Vassilev 2003
6	Greece	Ionian Coast	37.64N	21.32E	100	0.1	-36	Etiope et al 2013
7	China	Yinggehai Basin Hainan Is.	18N	109E	1	100	-36	Huang et al 2009
8	Australia	Timor Sea	13.8S	124.5E	474	0.7	-41.5	Brunskill et al 2011
9	Russia-Japan	NW shelf of Sea of Okhotsk	55N	145E	11000	730000	-49	Yoshida et al 2004
10	Chile	Mocha Island	38.2S	73.5W	815	3.1	-44	Jessen et al 2011
11	Romania-Ukraine	Northwest Black Sea	43 to 46N	28.5 to 34E	120000	250000	*-55*	Amouroux et al 2002
12	Russia	East Siberian Arctic Shelf	70 to 78N	120 to 180E	2000000	2000000	-63	Berchet et al 2016
13	Alaska-Canada	Beaufort Sea	70 to 72N	140 to 155W	50000	476000	-60	Lorenson et al 2016
14	Norway	Svalbard margin	74 to 79 N	7 to 10E	1500	201600	-55	Mau et al 2017
15	China-Brunei	South China Sea	3 to 25N	104 to 120E	175700	?	-9999	Tseng et al 2017
16	The Netherlands	North Sea - Dutch Dogger Bank	55° 20' N	4° 05' E	-9999	8	-60	Romer et al 2017
17	USA	North US Atlantic margin	35 to 41 N	75 to 65 W	-9999	94000	*-60*	Skarke et al 2014
18	Pakistan	Makran offshore	24° N	62° E	-9999	50	-68	Romer et al 2012
19	USA - Mexico	Gulf of Mexico	*whole coastal zone*		-9999	200000	*-50*	Kennicutt 2017
20	Italy	Adriatic Sea, Marche (Fontespina)	43.33 N	13.72 E	-9999	0.5	-55	Etiope et al 2014
21	Italy	Adriatic Sea, Veneto (Chioggia)	45.2 N	12.3 E	-9999	0.1	*-65*	Panieri 2006
22	France	Aquitaine shelf (Bay of Biscay)	43°57' to 44° 2	2° 5' to 2° W	-9999	400	-69	Ruffine et al. 2017
23	USA	Monterey Bay	37	122.25	-9999	700	-31	Mullins and Nagel 1982
24	USA	Cape Lookout Bight N.Carolina	34.65	76.54 W	-9999	1	*-65*	Martens and Klump 1980
25	USA	Delaware Bay	39	75 W	-9999	10	*-65*	Moody and Van Reenan 1967
26	Canada	Laurentian Channel	48.00 N	65.00 W	-9999	1	-9999	Fader 1991
27	Canada	Grand Banks Downing Basin	46.8 N	56.6 W	-9999	1	-9999	Fader 1991
28	Greece	Patras Gulf	38.15 N	21.35 E	-9999	1	*-65*	Papatheodorou et al 1993
29	Russia	East Kamtchatka shelf	56 N	162.50 E	-9999	60	-9999	Seliverstov et al 1994
30	Denmark	West Bornholm, S. Baltic Sea	55.30 N	15 E	-9999	10	*-65*	Kogler and Larsen 1979
31	Azerbaijan-Turkmenistan	Caspian Sea	37.9 to 40.2N	49.4 to 51.7E	-9999	40000	*-49*	Yusifov and Rabinowitz 2004

Note: δ^{13}C values in *italic* are theoretically attributed (see main text). In the grid text files, the value -9999 for δ^{13}C is replaced by the emission-weighted average δ^{13}C value resulting from the first 15 seepage zones (-59 ‰).

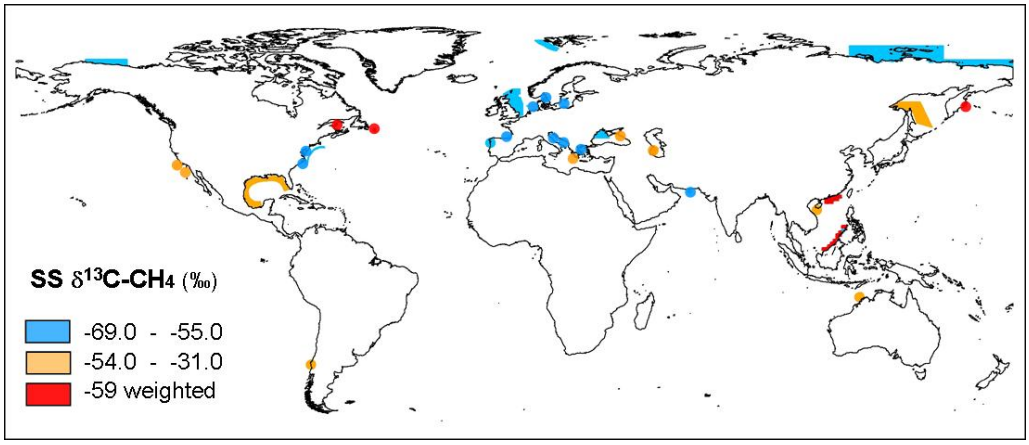

Fig. S5 Microbial (blue) and thermogenic (yellow) CH_4 attributed to the SS areas. Red refers to the areas where, lacking measured or estimated isotopic data, the global weighted-average SS isotopic value is used. See Fig.5 for the identification of the sites.

S3. Microseepage (MS)

S3.1 Global petroleum field area (PFA)

The spatial distribution of petroleum fields is taken from the "Petrodata" dataset of Päivi et al. (2007; see Sources of datasets in the Supplement). This dataset includes 891 polygons that represent onshore oil and gas fields from 114 countries. Päivi et al. (2007) created the polygons by grouping proximate original oil and gas locations digitised by geo-referenced maps (from USGS, 2000) in order to represent the clusters. The construction of the polygons was realised by applying a buffer of 30 km around each point location (i.e. this method assumes that each data point represents an area with a 30 km radius); overlapping polygons were then dissolved (to obtain one polygon) and clipped by using the country borders. The reasons why Päivi et al. (2007) used a 30 km buffer are not clear. We have compared the area of the Petrodata polygons with the actual area of petroleum fields mapped (PFM) in six main petroliferous regions: Siberia, USA, Iran, Venezuela, Turkmenistan and Iraq-Saudi Arabia. Gas and oil fields were digitized from geo-referenced maps published by different sources. We observed that the polygonal area of petroleum fields (resulting from the 30 km buffer) is, on average, 40% higher than the actual petroleum field area reported in the specific maps. We have then re-sized the polygons:

- using the observed polygon/PFM ratio for each of the 6 regions used as test (variable from 0.9 to 6.8),
- using the average polygon/PFM ratio (1.67) for all other fields.

This process resulted in a global Petroleum Field Area (PFA; Fig. S6) of 13,033,755 km^2 (about 9.7 million km^2 , i.e. ~43%, smaller than the area derivable from the polygons of Päivi et al. 2007).

S3.2 Global area including macro-seeps outside PFA (OS area, OSA)

The existence of macro-seeps (OS) in a given region implies a high probability that the region is also characterized by diffuse MS, which is not directly related to the gas flow of specific seeps (i.e., it is not a halo surrounding the macro-seeps, a process called miniseepage; Etiope, 2015). MS would occur, in other words, in areas surrounding OS and within OS clusters, regardless the presence of petroleum fields (we have in fact verified that 779 OS fall outside the PFA). We call this area of influence "OS area - OSA". The OSA was built creating a buffer of 5 km (radius) around each OS that falls outside PFA and enveloping OS clusters. The resulting global OSA is 85,900 km^2. The radius of 5 km reflects the average distance between seeps within small-scale clusters, and covers therefore the minimum area where seepage may occur. The average distance between seeps was calculated using the nearest neighbor index (NNI) for 16 OS clusters in different regions. Cluster identification was based on Hot Spot Analysis by using Zonal Nearest Neighbor Hierarchical spatial clustering (ZNNH). The total potential MS area (PMA) is therefore PFA+OSA = 13,033,000 + 85,900 = 13,118,900 km^2.

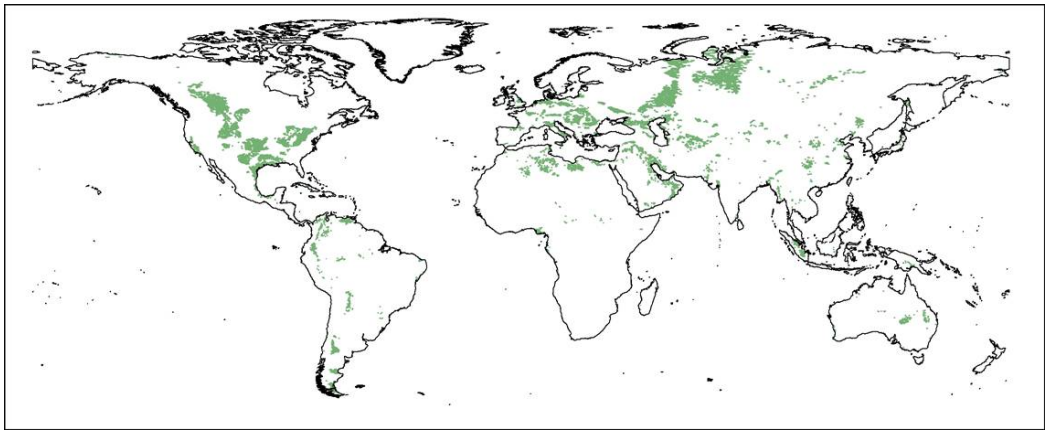

Fig. S6 Global distribution of the petroleum field area (PFA), based on "Petrodata" dataset from Päivi et al. (2007)

Table S5. Statistics of microseepage data (values are in mg m^{-2} d^{-1})

	N.	Mean	Median	G.Mean	Min	Max	Std.Dev.
Total	1509	111.8	0.20	-	-40.99	7078.7	548.8
Positive flux (>0.01)	871	194.8	2.73	4.02	0.01	7078.7	711.1

G.Mean: geometric mean; Min: minimum value; Max: maximum value, Std.Dev.:, standard deviation

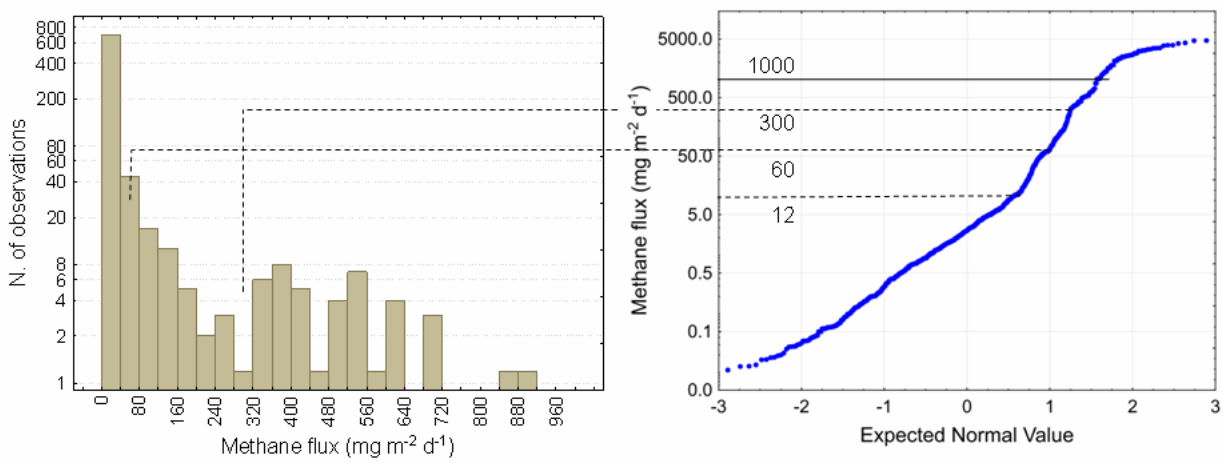

Fig. S7 Statistical elaboration of the microseepage data from Table S5.

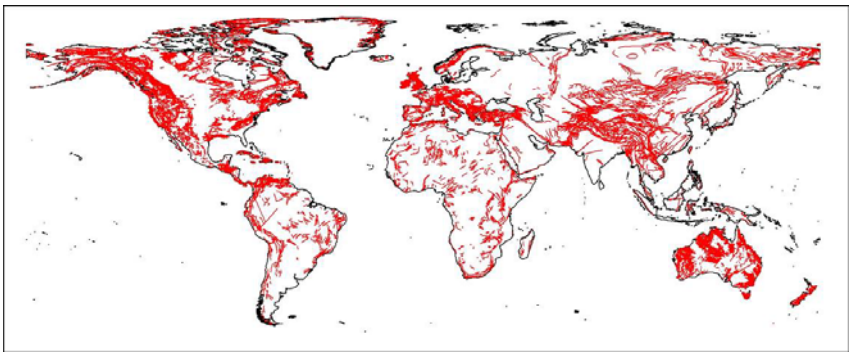

Fig. S8 Global distribution of major fault zones (see Sources of databases below)

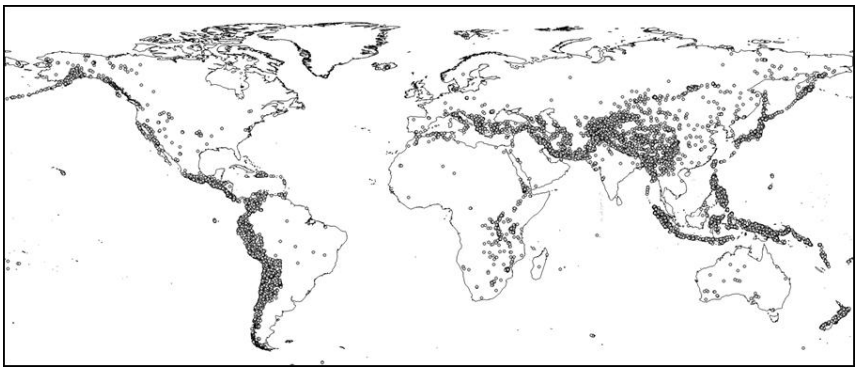

Fig. S9 Global distribution of earthquakes (period 2005-2017, M>4.5) (see Sources of databases below)

Table S6. Results of microseepage gridding (0.05° x 0.05°)

	N. cells	Area (km^2)	MS ($mg\ m^{-2}\ d^{-1}$)	MS ($tonnes\ km^{-2}\ y^{-1}$)	Tot output (tonnes year-1)
Gridded EMA	192,166	8,588,634			**24,006,755**
Gridded Level 1	169,338	7,652,785	1.3	0.4745	3,631,246
Gridded Level 2	20,518	840,772	31.14	11.366	9,556,200
Gridded Level 3	1094	45,059	110	40.15	1,809,156
Gridded Level 4	1216	50,016	493.5	180.13	9,010,153

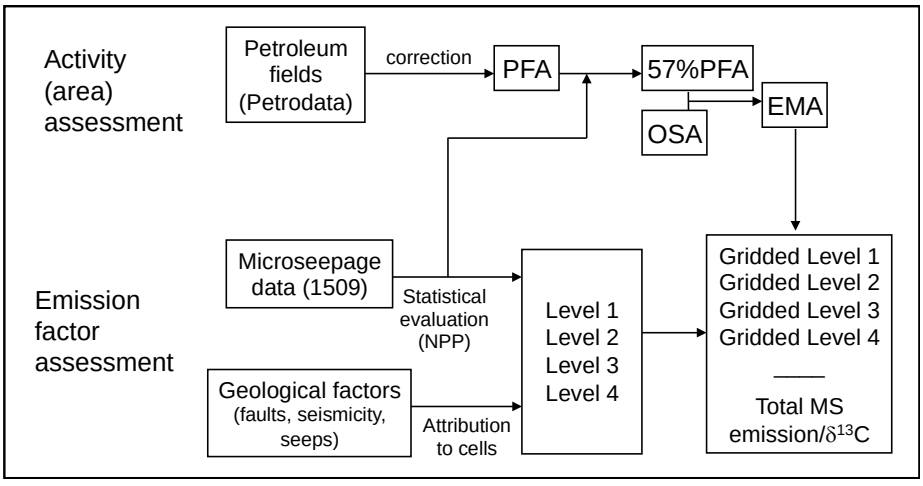

Fig. S10 Block diagram of the MS modeling. PFA: Petroleum Field Area; OSA: Onshore Seep Area; EMA: Effective Microseepage Area; NPP: Normal Probability Plot (see also explanation of the abbreviations in Section 6.1)

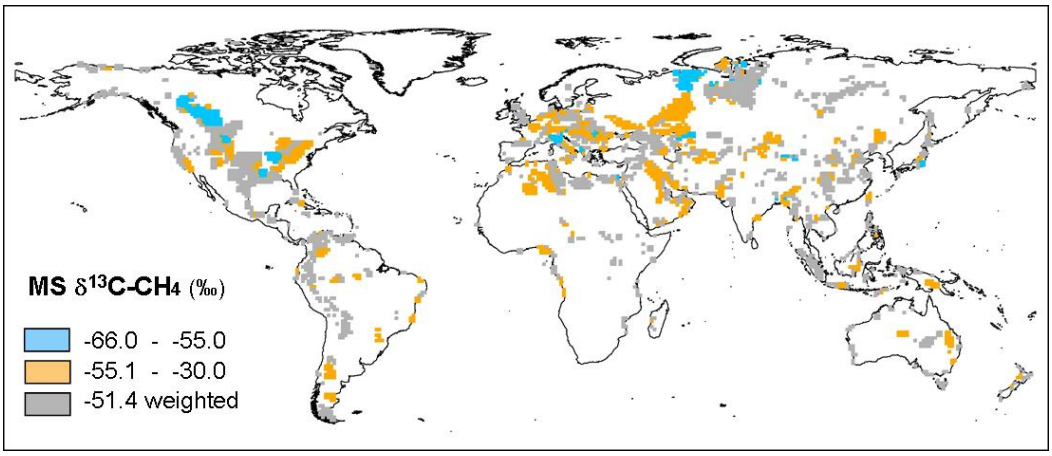

Fig. S11 Gridded map of MS methane $\delta^{13}C$ values. This map refers to the csv file "MS_13C"

S3.3 MS modeling sensitivity

The sensitivity of the MS modeling was checked by changing the emission factor (using the geometric mean of MS levels, instead of the median; varying the four microseepage levels by the 95% confidence interval for the median) and activity (varying ± 20% the area of the four levels). The several combinations and results are summarized in Table 7. The resulting emissions range from ~15 to ~32.7 Tg year^{-1}, with an average of 23 Tg year^{-1}, which matches the first estimate (combination n. 1 in Table S7) considered for the text file.

Table S7. Variability of the MS modeling results in relation to different combinations of activity and emission factors

Combination n.	Activity	Emission factor	Total emission (Tg year^{-1})
1	EMA	median	24.0
2	EMA	geom. median	21.9
3	EMA 20% smaller	median	18.9
4	EMA 20% smaller	geom. mean	17.5
5	EMA 20% higher	median	28.4
6	EMA 20% higher	geom. mean	26.3
7	EMA	lower 95% confid. limit median	18.8
8	EMA	upper 95% confid. limit median	27.3
9	EMA 20% smaller	lower 95% confid. limit median	15.0
10	EMA 20% higher	upper 95% confid. limit median	32.7

4. Geothermal manifestations (GM)

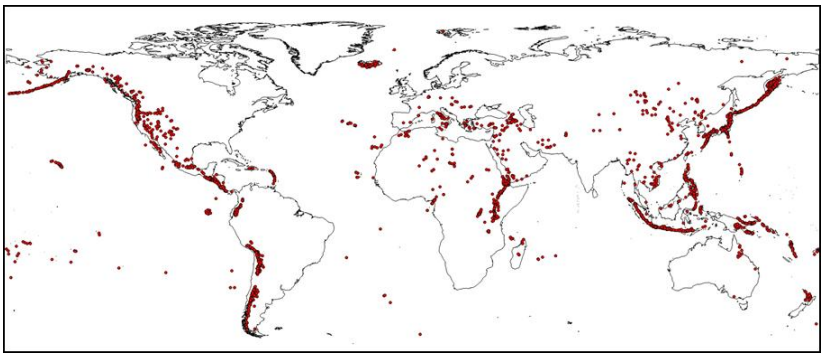

Fig. S12 Global distribution of onshore volcanic and geothermal sites (see Sources of databases below)

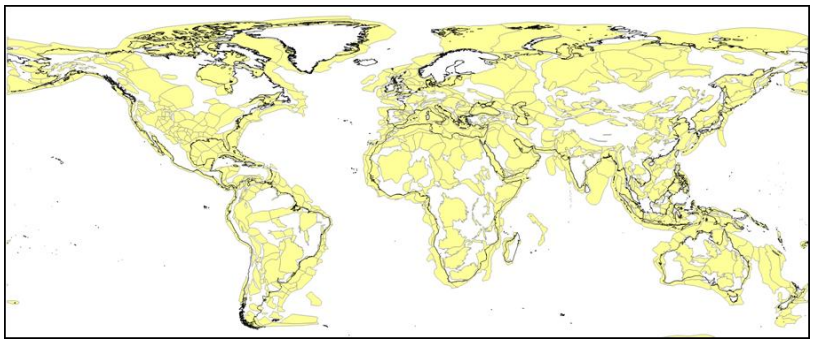

Fig. S13 Map of sedimentary basins (see Sources of databases below)

Table S8. Descriptive statistical data of GM $\delta^{13}C\text{-}CH_4$ values (‰)

	N.	mean	min	max	Std. Dev.
GM outside sedimentary basins	68	-24.3	-28.9	-16.6	3.6
GM within sedimentary basins	26	-32.3	-38	-29.1	2.9

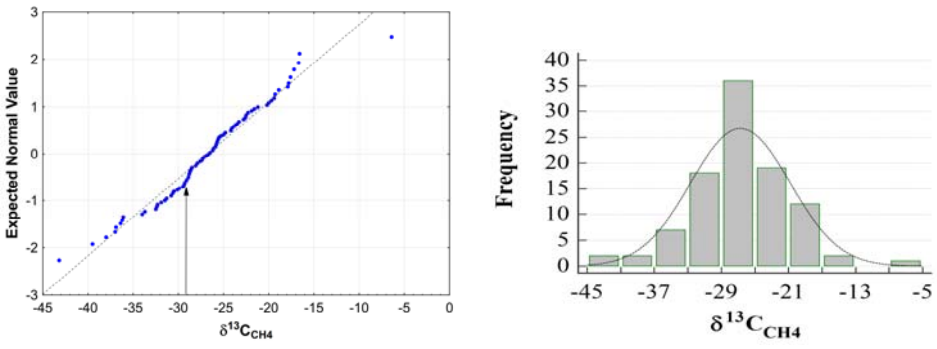

Fig. S14 Normal Probability Plot and frequency histogram of the GM $\delta^{13}C\text{-}CH_4$ data

Table S9. Results of GM gridding

	Emission level (tonnes year^{-1})	N. sites	N. cells	Tot output (tonnes year^{-1})
GM outside sedimentary basins	500	1513	526	1,636,500
GM within sedimentary basins (outside petroleum basins)	5000	832	409	3,761,205
GM within petroleum basins	10000	33	24	310,500
Total		2378	959	5,708,205

S5. Supplementary references

Amouroux, D., Roberts, G., Rapsomanikis, S., and Andreae, M.O.: Biogenic gas (CH_4, N_2O, DMS) emission to the atmosphere from near-shore and shelf waters of the north-western Black Sea. Estuar. Coast. Shelf Sci, 54, 575–587, 2002.

Berchet, A., Bousquet, P., Pison, I., Locatelli, R., Chevallier, F., Paris, J.-D., Dlugokencky, E. J., Laurila, T., Hatakka, J., Viisanen, Y., Worthy, D. E. J., Nisbet, E., Fisher, R., France, J., Lowry, D., Ivakhov, V., and Hermansen, O.: Atmospheric constraints on the methane emissions from the East Siberian Shelf, Atmos. Chem. Phys., 16, 4147–4157, 2016.

Brunskill, G.J., Burns, K.A., and Zagorskis, I.: Natural flux of greenhouse methane from the Timor Sea to the atmosphere, J. Geophys. Res., 116, G02024, doi:10.1029/2010JG001444, 2011.

Dando, P.R., Jensen, P., O'Hara, S.C.M., Niven, S.J., Schmaljohann, R., Schuster, U., and Taylor, L.J.: The effects of methane seepage at an intertidal/shallow subtidal site on the shore of the Kattegat, Vendsyssel, Denmark, Bull. Geol. Soc. Den., 41:65–79, 1994.

Dimitrov, L., and Vassilev, A.: Black Sea gas seepage and venting structures and their contribution to atmospheric methane. Annual of Univ. of mining and geology ''St.Ivan Rilski'', 46, part I. Geology and Geophysics, Sofia, 331-336, 2003.

Etiope, G., and Feyzullaiev, A., Baciu, C.L., and Milkov, A.V.: Methane emission from mud volcanoes in eastern Azerbaijan. Geology, 32, 6, 465-468, 2004a.

Etiope, G., Baciu, C., Caracausi, A., Italiano, F., and Cosma, C.: Gas flux to the atmosphere from mud volcanoes in eastern Romania, Terra Nova, 16, 179-184, 2004b.

Etiope, G., Christodoulou, D., Kordella, S., Marinaro, G., and Papatheodorou, G.: Offshore and onshore seepage of thermogenic gas at Katakolo Bay (Western Greece), Chem. Geol., 339, 115-126, 2013.

Etiope, G., Martinelli, G., Caracausi, A., and Italiano F.: Methane seeps and mud volcanoes in Italy: gas origin, fractionation and emission to the atmosphere, Geoph.Res.Lett., 34, L14303, doi: 10.1029/2007GL030341, 2007.

Etiope, G., Nakada, R., Tanaka, K., and Yoshida, N.: Gas seepage from Tokamachi mud volcanoes, onshore Niigata Basin (Japan): origin, post-genetic alterations and CH_4-CO_2 fluxes, Applied Geochemistry, 26, 348-359, 2011.

Etiope, G., Panieri, G., Fattorini, D., Regoli, F., Cannoli, P., Italiano, F., Locritani, M., and Carmisciano, C.: A thermogenic hydrocarbon seep in shallow Adriatic Sea (Italy): gas origin, sediment contamination and benthic foraminifera, Mar. Petrol.Geol., 57, 283-293, 2014.

Fader, G.B.: Gas-related sedimentary features from eastern Canadian continental shelf, Cont. Shelf Res., 11, 1123-1153, 1991.

Frunzeti, N., Baciu, C., Etiope, G., and Pfanz, H.: Geogenic emission of methane and carbon dioxide at Beciu mud volcano (Berca-Arbanasi hydrocarbon-bearing structure, Eastern Carpathians, Romania), Carpathian J. Earth Envir. Sci., 7, 159-166, 2012.

Garcia-Gil, S.: A natural laboratory for shallow gas: the Rıas Baixas (NW Spain), Geo-Marine Letters 23, 215-229, 2003.

Hong, W.L., Etiope, G., Yang, T.F., and Chang, P.Y.: Methane flux of miniseepage in mud volcanoes of SW Taiwan: Comparison with the data from Europe, J. Asian Earth Sci., 65, 3-12, 2013.

Hornafius, J.S., Quigley, D., and Luyendyk, B.P.: The world's most spectacular marine hydrocarbon seeps (Coal Oil Point, Santa Barbara Channel, California): quantification of emissions, J. Geophys. Res. 20(C9), 20,703–20,711, 1999.

Huang, B., Xiao, X., Li, X., and Cai, D.: Spatial distribution and geochemistry of the nearshore gas seepages and their implications to natural gas migration in the Yinggehai Basin, offshore South China Sea, Mar. Petrol. Geol., 26, 928-935, 2009.

Jessen, G.L., Pantoja, S., Gutierrez, M.A., Quiñones, R.A., Gonzalez, R.R., Sellanes, J., Kellermann, M.Y., and Hinrichs, K.-U.: Methane in shallow cold seeps at Mocha Island off central Chile, Cont. Shelf Res. 31, 574–581, 2011.

Judd, A.G., Davies, J., Wilson, J., Holmes, R., Baron, G., and Bryden, I.: Contributions to atmospheric methane by natural seepages on the UK continental shelf, Mar. Geol., 137, 165–189, 1997.

Kennicutt, M.C.: Oil and Gas Seeps in the Gulf of Mexico, In: Ward C. (eds) Habitats and Biota of the Gulf of Mexico: Before the Deepwater Horizon Oil Spill. Springer, New York, NY, 2017.

Kögler, F.C., and Larsen, B.: The West Bornholm Basin in the Baltic Sea: geological structure and Quaternary sediments, Boreas, 8, 1-22, 1979.

Lorenson, T.D., Grienert, J., and Coffin, R.B.: Dissolved methane in the Beaufort Sea and the Arctic Ocean, 1992–2009; sources and atmospheric flux, Limnol. Oceanogr., 61, 300-323, 2016.

Martens, C.S., and Klumo, J.V.: Biogeochemical cycling in an organic rich coastal marine basin. 1. Methane sediment-water exchange processes, Geochim. Cosmochim. Acta, 44, 471-490, 1980.

Mau, S., Römer, M., Torres, M.E., Bussmann, I., Pape, T., Damm, E., Geprägs, P., Wintersteller, P., Hsu, C.-W., Loher, M., and Bohrmann, G.: Widespread methane seepage along the continental margin off Svalbard - from Bjørnøya to Kongsfjorden, Sci. Reports, 7, 42997, DOI: 10.1038/srep42997, 2017.

Moody, D.W., and Van Reenan E.D.: High-resolution subbottom seismic profiles of the Delaware Estuary and Bay mouth, US Geol. Surv. Prof. Pap. 575-D, D247-D252, 1967.

Mullins, H.T., and Nagel, D.K.: Evidence for shallow hydrocarbons offshore northern Santa Cruz County, California, AAPG Bull., 66, 1130-1140, 1982.

Panieri, G.: Foraminiferal response to an active methane seep environment: a case study from the Adriatic Sea, Mar. Micropaleontol., 61, 116-130, 2006.

Papatheodorou, G., Hasiotis, T., and Ferentinos, G.: Gas-charged sediments in the Aegean and Ionian Seas, Greece, Mar. Geol. 112, 171–184, 1993.

Römer, M., Sahling, H., Pape, T., Bohrmann, G., and Spieß V.: Quantification of gas bubble emissions from submarine hydrocarbon seeps at the Makran continental margin (offshore Pakistan), J. Geophys. Res., 117, C10015, doi:10.1029/2011JC007424, 2012.

Romer M., Wenau S., Mau S., Veloso M., Greinert J., Schl€uter M., Bohrmann G.: Assessing marine gas emission activity and contribution to the atmospheric methane inventory: A multidisciplinary approach from the Dutch Dogger Bank seep area (North Sea), Geochem. Geophys. Geosyst., 18, 2617–2633, doi:10.1002/2017GC006995, 2017.

Ruffine, L., Donval, J.P., Croguennec, C., Bignon, L., Birot, D., Battani, A., Bayon, G., Caprais, J.C., Lantéri, N., Levaché, D., and Dupré, S.: Gas Seepage along the edge of the Aquitaine Shelf (France): origin and local fluxes. Geofluids, 2017, doi:10.1155/2017/4240818, 2017.

Skarke, A., Ruppel, C., Kodis, M., Brothers, D., and Lobecker, E.: Widespread methane leakage from the sea floor on the northern US Atlantic margin. Nature Geosci., DOI: 10.1038/NGEO2232, 2014.

Spulber, L., Etiope, G., Baciu, C., Malos, C., and Vlad, S.N.: Methane emission from natural gas seeps and mud volcanoes in Transylvania (Romania), Geofluids, 10, 463-475, 2010.

Seliverstov, N.I., Torokhov, P.I., Egorov, Y.O., Dubrovsky, V.N., Taran, Y.A., and Kokarev, S.G.: Active seeps and carbonates from the Kamchatsky Gulf (East Kamchatka), Bull. Geol. Soc. Denmark, 41, 50-54, 1994.

Tizzard, L.H.: The contribution to atmospheric methane from sub-seabed sources in the UK continental shelf, Unpublished Ph.D. Thesis, University of Newcastle upon Tyne, UK, 329pp, 2008.

Tzeng, H.C., Chen, C.T.A., Borges, A., DelValls, A., and Chang Y.C.: Methane in the South China Sea and the Western Philippine Sea, Contin. Shelf Res., 135, 23-34, 2017.

Yoshida, O., Inoue, H.Y., Watanabe, S., Noriki, S., and Wakatsuchi, M.: Methane in the western part of the Sea of Okhotsk in 1998–2000, J. Geophys. Res., 109, C09S12, doi:10.1029/2003JC001910, 2004.

Yusifov, M., and Rabinowitz, P.D.: Classification of mud volcanoes in the South Caspian Basin, offshore Azerbaijan, Mar. Pet. Geol., 21, 965–975, 2004.

Zheng, G., Ma, X., Guo, Z., Hilton, D.R., Xu, W., Liang, S., Fan, Q., and Chen, W.: Gas geochemistry and methane emission from Dushanzi mud volcanoes in the southern Junggar Basin, NW China, J. Asian Earth Sci., 149, 184-190, 2017.

S6. Sources of databases

Faults

Global. Finko (2014). Global Faults layer from ArcAtlas (ESRI).
http://www.arcgis.com/home/item.html?id=a5496011fa494b99810e4deb5c618ae2#overview

Afghanistan. Dep. of the Interior, Data.gov team https://catalog.data.gov/dataset/geologic-faults-of-afghanistan-fltafg

Australia. Geoscience Australia and Australian Stratigraphy Commission. (2017). Australian Stratigraphic Units Database. http://www.ga.gov.au/products-services/data- applications/reference-databases/stratigraphic-units.html

Bangladesh. Dep. of the Interior, Data.gov team, https://catalog.data.gov/dataset/faults-and-tectonic-contacts-of-bangladesh-flt8bg

Caribbean Region. Dep. of the Interior, Data.gov team https://catalog.data.gov/dataset/faults-of-the-caribbean-region-flt6bg

Central Asia. Mohadjer, S., Strube, T., Ehlers, T.A., Bendick, R., 2015, Central Asia Fault Database. Available at esdynamics.geo.uni-tuebingen.de/faults/[02/15/18]

Europe including Turkey. Dep. of the Interior, Data.gov team https://catalog.data.gov/dataset/faults-of-europe-including-turkey-flt4-2l

Georgia. Gamkrelidze I., Gamkrelidze M., Loladze M., Tsamalashvili T., 2000. New Tectonic Map of Georgia (Explanatory Note). Bull. Georgian Nat. Acad. Sci., vol. 9, no. 1, 201

Greece. Basili R., Kastelic V., Demircioglu M. B., Garcia Moreno D., Nemser E. S., Petricca P., Sboras S. P., Besana-Ostman G. M., Cabral J., Camelbeeck T., Caputo R., Danciu L., Domac H., Fonseca J., García-Mayordomo J., Giardini D., Glavatovic B., Gulen L., Ince Y., Pavlides S., Sesetyan K., Tarabusi G., Tiberti M. M., Utkucu M., Valensise G., Vanneste K., Vilanova S., Wössner J. (2013). The European Database of Seismogenic Faults (EDSF) compiled in the framework of the Project SHARE. *http://diss.rm.ingv.it/share-edsf/*, doi: 10.6092/INGV.IT-SHARE-EDSF.

Iran. Dep. of the Interior, Data.gov team https://catalog.data.gov/dataset/major-faults-in-iran-flt2cg
Ireland: Geological Survey Ireland, Ireland www.gsi.ie, November 2016

Ireland. Geological Survey Ireland, www.gsi.ie, November 2016

Italy. Elementi tettonici presenti nella Carta Geologica d'Italia alla scala 1:100.000. Proprietà del: Servizio Geologico d'Italia – ISPRA. Portale del Servizio geologico d'Italia, e metti il link del portale stesso http://sgi.isprambiente.it/geoportal/

New Zealand. GNS Science, http://data.gns.cri.nz/af/ New Zealand Active fault database
South America: Veloza G., Styron R., Taylor M.. (2013). Active Tectonics of the Andes database (ATA)

South America. Veloza, G., Styron, R., Taylor, M., Mora, A., 2012, Active Tectonics of the Andes: An open-source archive for active faults in northwestern South America, GSA Today, 22, 4-10, doi: 10.1130/GSAT-G156A.1.
https://github.com/ActiveTectonicsAndes/ATA

Spain. IGME (2015). QAFI v.3: Quaternary Active Faults Database of Iberia. Accessed "February 2018", http://info.igme.es/QAFI

Switzerland. Opendata.swiss, 2005. Mappa tettonica della Svizzera (GK500-Tekto). Ufficio federale di topografia. http://opendata.swiss/themes/geography.

United Kingdom. British Geological Survey, BGS Geology 625k (DiGMapGB-625) data 1: 625 000 ESRI® [Faults].
http://www.bgs.ac.uk/products/digitalmaps/dataInfo.html#_625

Earthquakes

USGS Earthquake Lists, Maps and Statistics (https://earthquake.usgs.gov/earthquakes/browse/

Sedimentary basins

Sedimentary basins world map (CGG data services)
http://www.datapages.com/gis-map-publishing-program/gis-open-files/global-framework/robertson-tellus-sedimentary-basins-of-the-world-map

Petroleum fields

“Petrodata” from Päivi et al. (2007) by PRIO (Peace Research Institute Oslo), http://www.prio.org

Volcanoes/geothermal sites

Global Volcanism Program (2013) http://www.volcano.si.edu/